

An Experimental Investigation of the Impact Response and Post-impact Shear Buckling Behaviour of Hybrid Composite Laminates

Mahdi Damghani ^{a,*}, John Saddler ^a, Ethan Sammon ^a, Gary A. Atkinson ^a, Jason Matthews ^a, Adrian Murphy ^b

^a Department of Engineering Design and Mathematics (EDM), University of the West of England (UWE), Bristol, BS16 1QY, UK

^b School of Mechanical and Aerospace Engineering, Queen's University Belfast (QUB), Belfast, BT9 5AG, UK

Abstract

This paper investigates the effect of transverse impact loading on the in-plane shear behaviour of two laminate configurations. The extensive experimental studies consider a pure carbon laminate (type 1) and a novel X-shaped carbon/glass laminate (type 2). The results establish that **all three graduated** impact energy levels **(5J, 7.5J and 10J)** induce through-thickness matrix cracking, fibre breakage and delamination in the type 1 laminate. However, the use of glass plies in the type 2 laminate resulted in only matrix cracking towards the impacted surface and limited through-thickness damage. Post impact, both laminate types demonstrated lower buckling load, failure load and stiffness. The reduction in buckling load of the type 1 specimens was greater than that of the type 2 specimens. However, the reduction in failure load of the type 1 specimens was less than that seen in the type 2 specimens. Both laminate types demonstrated a stable post-buckling equilibrium path. A novel machine vision technique based on polarisation imaging was successful in standardising the process of identifying the

* Corresponding author. Tel.: +4411732 87369
Email address: Mahdi.Damghani@uwe.ac.uk

damage location/size for the type 1 laminates, but not for the type 2 laminates. This was due to the inclusion of surface glass plies which, unlike carbon plies, do not polarise light at the point of reflection.

Keywords: Composite laminates, Low velocity impact, Shear loading, Impact behaviour

1 Introduction

Laminated Carbon Fibre Reinforced Polymers (CFRP) and Glass Fibre Reinforced Polymers (GFRP) are increasingly being used in aerospace, automotive, renewable energy, marine and defence products. This is due to their high strength and stiffness to weight ratio, corrosion resistance and enhance fatigue performance compared to conventional isotropic materials [1]. However, due to fibre brittleness and lack of through thickness reinforcements, CFRP and GFRP laminates are susceptible to damage resulting from out-of-plane loading such as that caused by transverse impact [2]–[5].

CFRP and GFRP laminates may experience impact loading during manufacture and/or while in service. For example, for aerospace products the source of in-service damage could be: accidental tool drop during aircraft maintenance; tyre burst and debris impact when taking off or landing; accidental damage during taxiing; bird, hailstone, or lightning strikes. Each impact type may have a wide range of energies, leading to a correspondingly wide range of damage types and magnitudes. It is generally understood that impact energy levels of less than 50 J can lead to Barely Visible Impact Damage (BVID) [6], [7]. BVID is small at the exposed laminate surface but has the potential to be larger below the surface, with damage such as subsurface delaminations, matrix cracks and/or fibre damage. The combination of each damage

form is dependent on the impact energy, boundary conditions, aspect ratio and stacking sequence of the laminate. As such, BVID may not be found during general visual inspection and in aerospace design BVID is thus assessed considering ultimate loads (aircraft ultimate load is often 1.5 times the limit load, i.e. load beyond which the structure will fail).

With higher impact energies (typically $\geq 50 J$) Visible Impact Damage (VID) occurs. VID has significant visible fibre breakage, which is typically in addition to delaminations and transverse shear cracking. The magnitude of delamination also increases through the thickness [8], [9]. Generally, aerostructures are assessed under limit load for VID. It is well established in the literature that both BVID and VID lead to a substantial reduction in composite material load bearing capacity (by more than 70%) when under the action of compressive, tensile and/or shear force loading [10]. Much work has been undertaken to build understanding of both the impact damage and the post impact strength of laminates [11]. To date, the majority of work has focused on laminates made of a single material (i.e. pure carbon or glass) system and subject to in-plane compressive or tensile loading post impact only [12]–[14]. Significantly less research is available on hybrid laminates, containing *both* carbon and glass plies where individual plies are shaped within the stacking sequence, i.e. individual plies within the stack are cut into shapes which do not match the overall laminate dimensions. There is very little work which considers such novel laminate designs subject to shear loading once damaged. However, the limited work which is available does suggest that the hybridization and the shaping of individual plies could influence both the impact damage and the damaged laminate strength [11].

Thus, the aim of this paper is to investigate how impact damage and post impact shear buckling and post-buckling behaviour **after three graduated impact energies (5J,**

7.5J and 10J) vary with impact energy and understand the influence of hybridisation and X-braced ply shaping on this behaviour [11]. Herein, an extensive experimental study is undertaken to investigate and compare the behaviour of two rectangular laminates. The first laminate design has only woven carbon plies and all plies are uniform in the laminate in-plane orientation (type 1). The second laminate design uses both carbon/glass plies and a number of the carbon plies are X-shaped in the laminate in-plane orientation (type 2).

2 Background

This section introduces the current state of the art in the behaviour of laminates when subjected to impact loading and approaches to mitigate the associated effects on structural performance. Due to the abundance of work in this field, the review focuses on recent work (last five years) and on Compression After Impact (CAI), Tension After Impact (TAI) and Shear After Impact (SAI).

2.1 CAI behaviour

The majority of research in the literature is on CAI with CFRP and GFRP the most common laminate materials considered. CAI is most often studied as it is deemed to be more severely affected compared to TAI and SAI. The reduction in load bearing capacity in compression is often associated with either a reduction in material strength or a decreased global and/or local (sublaminate) buckling capacity. The current standard measure of CAI assessment is ASTM D 7137 [15]. Sun et al. [16] studied the CAI of two laminate configurations (ply-scaled and sublaminates-scaled) where damage was induced by low velocity impact. They observed that the sublaminates-scaled laminate had higher impact resistance compared to the ply-scaled cases leading to smaller delaminations for the same impact energy. The sublaminates-scaled laminate was also found to have a higher damage tolerance resulting from the

smaller delamination areas. The difference decreased as the damage size increased. In a similar work, Tuo et al. [17] reported impact damage and CAI performance considering impact energy increasing from 15 J to 45 J [16]. In their study, a direct correlation between reduction in compressive residual strength and increase in impact energy level was observed. Gliszczyński et al. [18] investigated compressive behaviour of channel sections made of GFRP material after 20 J and 30 J impact. It was observed that despite BVID and VID damage, each test sample followed a stable post-buckling equilibrium path. Zhang et al. [19] examined the CAI failure of tubular woven CFRP specimens with/without a Nomex honeycomb core. They reported the use of a core prevented impactor penetration and resulted in higher impact energy absorption, leading to more severe damage. Wu et al. [20] studied the effects of stacking sequences on the dynamic responses and damage mechanisms of ultra-high molecular weight polyethylene (UHMWPE) composites under multi-point low-velocity impact as well as the CAI behaviours. Three impact points, distributed in a triangular shape, were designed to represent random impact incidents.

It is concluded from the literature that CAI behaviour of CFRP and GFRP laminates is severely affected by low energy impacts ($\leq 50 J$). However, there is good understanding of how impact energy influences the form and scale of damage and how damage ultimately affects laminate strength under compression loading.

2.2 TAI behaviour

Literature on TAI behaviour is scarce, particularly in recent years. This is predominantly due to the notion that low velocity impact does not lead to fibre fracture and hence does not have a critical influence on the residual tensile strength. Moreover, it is widely accepted that delamination resulting from impact is less relevant to the residual tensile strength where fibres close to delaminations can still sustain significant

tensile loading [21]. However, low velocity impact could lead to splits in the off-axis plies that run from the free edge and join up via delamination to form a characteristic staircase pattern, providing a fracture path without necessarily involving fibre fracture [9]. It is worth noting that, despite the importance of TAI behaviour in many structural applications, unlike CAI, there are presently no recommendations and standards available in the literature.

Despite the overall small number of TAI papers, there are handful which examine hybrid laminates. Damghani et al. [7] impacted pure CFRP and hybrid CFRP-GFRP laminates with graduated energy levels (5 J, 7.5 J, 10 J). It was shown that hybridisation had the potential to contain the damage close to the impacted surface and inhibit the spread of damage through the thickness. Bogenfeld et al. [22] investigated impact damaged laminates under tension–fatigue loading. They reported slow and stable damage growth under tensile cyclic load for all their test samples. Experimental post-impact behaviour of thin woven CFRP and hybrid CFRP-GFRP under tensile cyclic loading was investigated by Rogani et al. [18], [19]. They established a correlation between stacking sequence and tension fatigue behaviour after impact. Although the use of a top GFRP layer reduced the impact damage size in the CFRP-GFRP laminates, fatigue damage initiated at the outer GFRP plies and then spread below into the CFRP plies. Dahil et al. [20] carried out experimental quasi-static tests of hybrid CFRP-GFRP laminates after V-notched Charpy impact test. It was found that notched specimens had on average less static strength compared to non-notched ones.

It is concluded from the literature that the examination of TAI behaviour is most often focused on the fatigue performance of composite structures. However,

hybridisation of CFRP with GFRP is often employed to decrease damage due to impact loading.

2.3 SAI behaviour

Like TAI, there is only limited literature on SAI behaviour. This is despite the fact that composite structures such as wing skin, ribs, spar webs and fuselage panels undergo significant in-plane shear load. Given the thin-walled nature of aerostructures, this could lead to premature buckling and affect post-buckling behaviour of such structures.

Feng et al. [23] studied the buckling and post-buckling performance of stiffened composite panels. The panels were studied with different impact damage positions but using only a fixed impact energy (50 J). It was shown that if the impact damage was not significant then stable buckling and failure load could be expected. However, for impact damage with fibre breakage, matrix cracks and de-bond of the skin-stiffener interface, the average reduction in buckling load could reach $\approx 22\%$ compared to the pristine panels. It is noteworthy that none of their impacted stiffened panels demonstrated buckling mode transition. In a later work [24], they extended the study and investigated the impact of damage evolution under fatigue load and SAI fatigue behaviours. They performed shear fatigue testing using tension-tension fatigue using a picture frame test fixture (stress ratio, $R = 0.1$, frequency, 2 Hz). It was observed that impact damage did not develop, deteriorate or enlarge during and after the fatigue loading. Additionally, the geometrical dimensions of the impact dents did not have obvious visible changes. However, the buckling and failure load of the panels had a relatively large drop after the impact treatment.

A comparative experimental and analytical study of circular cut-out and low-velocity impact (43 J and 19 J) on the damage resistance and damage tolerance of a thin GFRP plate was carried out by Oluwabusi et al. [25]. There was a 27% and a 25% reduction in post-buckling load of the circular cut-out and impacted specimens compared to the intact specimens, respectively. This could allude to the fact that impact damage may be represented as a circular/elliptical cut-out having similar impact damage size.

From the limited literature, it can be concluded that the residual shear strength, shear buckling and post-buckling load of composite structures are adversely affected because of impact damage. Given the few works in this domain, further work is required to bridge the gap in knowledge and understand structural behaviour under combined impact and shear loading.

2.4 Summary

In summary, fibre reinforced composite laminates must be designed considering impact loading and resulting damage. To date, most research works have considered single material laminates and compression loading. The behaviour of impact damaged laminates under tension and shear loading has received limited attention. However, fibre hybridisation and ply shaping could offer some immediate advantages under such loading conditions. There is a need to undertake focused experimental work and establish how impact damage and post-impact buckling and post-buckling behaviour varies with impact energy, particularly under shear loading. Also, there is not a current standard technique by which impact damage can be efficiently and quickly located on a large surface area during routine visual inspections of structures. This paper thus goes some way to address this side issue.

3 Materials and experimental methods

This section outlines laminates' dimensions and configurations, material properties used in the study, impact test set-up and post-impact shear test set-up using picture frame fixture.

3.1 Laminate designs

Two laminate types are investigated in this study based on designs obtained and studied in previous works [11], [26]. First, the type 1 laminates consisted of purely woven fabric CFRP plies with a quasi-isotropic stacking sequence $[\pm 45/\pm 45/0/0]_S$. In this laminate type, all CFRP plies had thickness 0.224 mm (see Table 1) and were square in shape with dimensions 200 mm \times 200 mm. This represents traditional or standard laminate design. The hybrid laminate design, labelled the type 2 laminate, includes both CFRP and GFRP plies, having a stacking sequence $[\pm 45G/\pm 45X/\pm 45X/0/0]_S$ where symbols X and G represent X -shaped CFRP ply and square GFRP ply, respectively. In this hybrid design the GFRP plies are located on the outer mould surfaces of the laminate. To compensate for the added weight of the GFRP plies, four of the CFRP plies are X shaped in the laminate in-plane orientation. The size of the X -shape CFRP plies were obtained via size optimisation study to yield a comparable shear buckling load with that of the type 1 laminate. It is worth noting that the thickness of each GFRP ply was 0.288 mm (see Table 1). The full details of this process are explained in [11] and hence not repeated in this work.

Figure 1 demonstrates the shape and orientation of each ply. It should be noted that, in a previous study [9], it was shown that scattering GFRP plies through the thickness improved impact performance more than clustering GFRP plies on the outer surfaces. However, the current aircraft wing designs require a sacrificial GFRP ply to be located at the outer mould surfaces whose stiffnesses are often ignored for

structural integrity assessments. As such, in this study, type 2 laminates with GFRP plies on the outer mould surfaces were adopted as opposed to scattering them through the laminate thickness to enable a more realistic study reflective of current industrial practice.

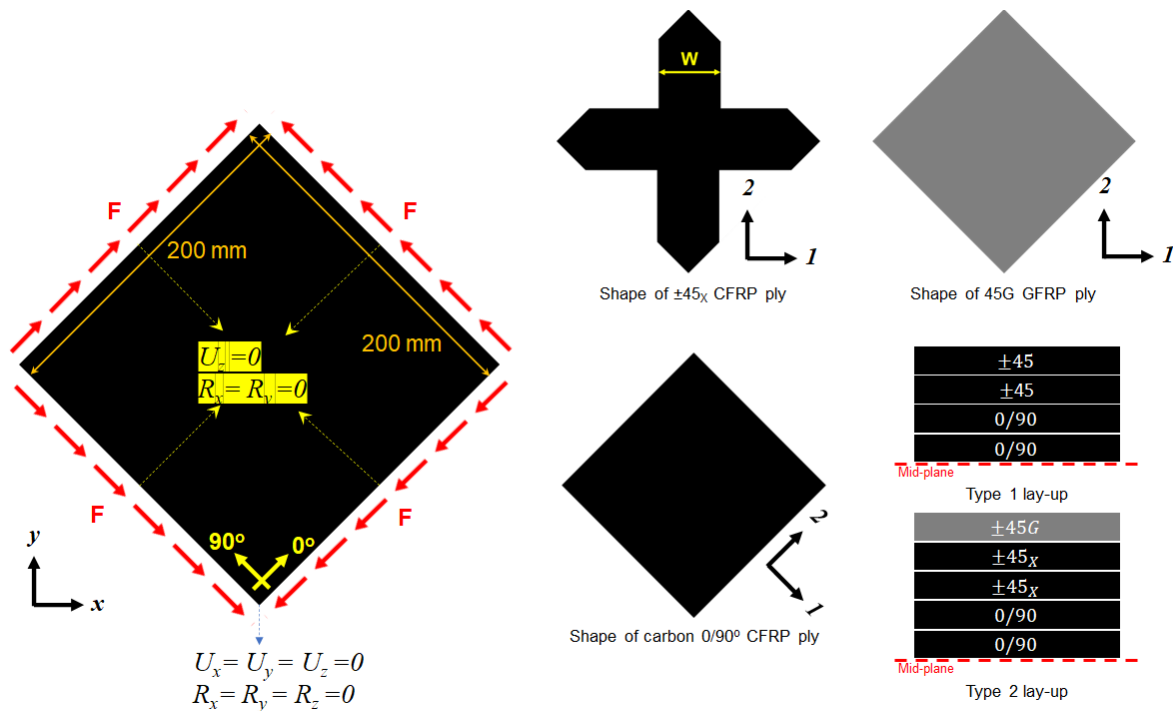


Figure 1: Loading, boundary conditions and ply shapes of the laminates (X and G represent X-shaped CFRP ply and GFRP ply, respectively)

3.2 Composite material and manufacture

CFRP and GFRP materials used in this study were woven twill pre-impregnated fabric AX-5180 and AX-3180, respectively, with the mechanical properties given in Table 1. Both carbon and glass prepreps consist of 54% fibre by volume (60% by weight) and have compatible resin contents enabling simultaneous hot press curing. Furthermore, the epoxy of the prepreg consists of 20% by weight of epoxy resin, 20% epoxy resin copolymers, and 20% flame retardant. The prepreg also encompasses 3% by weight of Fume silica, 3% Cyanoguanidine and 3% curing agent.

Twelve laminates of each type were manufactured. They were initially hand laid and cured in a heated press for one hour at 120°C and 100 *psi* pressure. They were then cut to size 200 *mm* × 200 *mm* for testing.

Table 1: Mechanical properties of woven CFRP (AX-5180) and GFRP (AX-3180) fabric plies [9], [11]

Mechanical properties	Units	AX-5180 CFRP	AX-3180 GFRP
$E_{11}=E_{22}$	MPa	67094.00	30083.00
G_{12}	MPa	4831.38	4954.60
S_t^*	MPa	595.50	437.16
S_c	MPa	393.00	306.00
S_s	MPa	87.00	62.00
Strain to failure	Strain	0.01	0.02
ν_{12} (Poisson's ratio)	N/A	0.04	0.14
t_{ply}^{**}	mm	0.224	0.288

* t, c and s subscripts denote the strength of ply in tensions, compression and shear respectively.

** cured ply thickness

3.3 Impact experiment

An in-house manufactured drop weight machine was used to conduct the impact experiments, with a blunt hemispherical shape impactor of 12.1 *mm* diameter. The impactor head and the guide mechanism had a combined mass of 1.82 *kg*. An additional, fixed mass of 1 *kg* was added to the impactor to give the impactor a total mass of 2.82 *kg*. In this study, three graduated impact energies were used, i.e. 5 *J*, 7.5 *J* and 10 *J*. The drop was determined by the potential energy equation $E_p = mgh$. E_p is the impact energy, m is the mass of the impactor, g is the acceleration due to gravity, and h is the drop height.

The set-up of the impact machine is shown in Figure 2. As shown in the figure, the laminates were placed on an aluminium base plate having a 50 *mm* diameter cut-out at the centre and then clamped at four corners. This configuration created a stiff support on the back face of the laminates. Evidently, the impact loading did not follow any impact standards such as that of ASTM D7136/D7136M-05 as the boundary conditions specified in the standard does not reflect all conditions experienced in

practice. The boundary conditions used are of interest where the laminate is supported or semi-supported on its back face. This could include additional structure or systems in contact with the structure. Finally, during the impact test, a digital data acquisition unit was used to record the impact force-time curve history at 10 kHz sampling frequency. It should be noted that the impact forces were calculated using a strain gauge-based load cell attached to the impact tower. The load cell was positioned under the fixture on which the test specimen was secured. In the load cell, the impact forces were converted into measurable electrical output. The data were recorded via PicoScope data logger and associated software. Then, the recorded electrical output (voltages) were converted into impact forces.

To extract energy-time histories from the recorded force-time histories of the impact, an analytical approach was taken. The energy at time t of the impact ($E(t)$) was obtained using the analytical formulation below

$$E(t) = \frac{mv_0^2}{2} - \frac{mv(t)^2}{2}$$

where v_0 and $v(t)$ are the velocities just before impact and at impact time t , respectively. It was assumed that the initial potential energy of the impact (5 J, 7.5 J and 10 J) was fully converted into kinetic energy just prior to the impact. Thus, v_0 could be expressed as

$$v_0 = \sqrt{\frac{2E_p}{m}}$$

Since the change in the momentum of impactor is equal to the impulse of impact force, the velocity at time t of the impact was calculated using

$$v(t) = v_0 + \frac{1}{m} \int F(t) dt$$

where $F(t)$ is the impact force at time t .

For each impact energy, four specimens of each laminate type were impacted at the centre. Thus, a total of twelve specimens for each laminate type were impacted. Nine of the impacted specimens were used in quasi-static mechanical testing (see section 3.5) and the other three were used for sectioning to study the damage form and scale after impact.

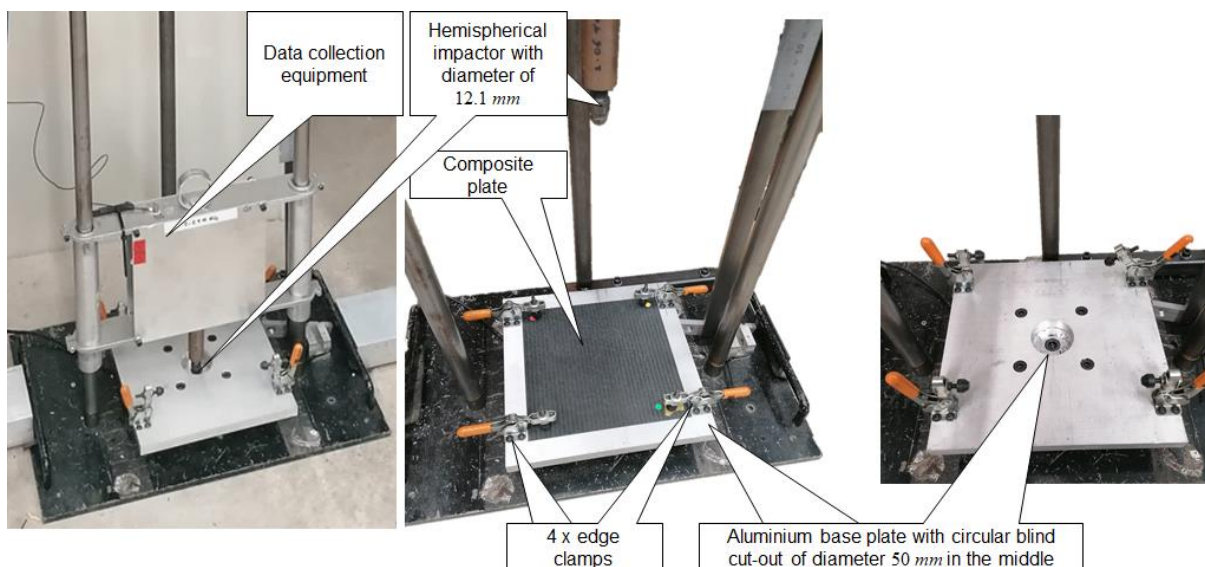


Figure 2: Impact test set-up

3.4 Damage after impact and machine vision

To obtain reliable surface geometric data of the damage in this paper, a novel machine vision technique is applied [27]. The approach uses a Sony XCG-CP510 camera with a 16 mm lens and an exposure time of 10 ms (for the carbon fibre laminates) and 2 ms (for the hybrid laminates). The impacted laminate and the camera was placed under a MBJ Imaging SDL-30-SDL-30 dome illuminator of light wavelength 465 nm to create uniform hemispherical illumination. As explained in Section 4 and

[28], the XCG-CP510 camera is sensitive to the polarisation state of incoming light. As a conductor, the carbon fibres naturally linearly polarise the light parallel to the fibres at the point of reflection. This polarisation can be visualised (in MATLAB for this paper) to aid in the detection of the visible external damage perimeter. This assists in inspection of the laminate as damage often manifests in the form of a disruption to fibre orientations. In this paper, images of damage were captured using the XCG-CP510 and points on the perimeter of damaged regions manually selected. For the front side for type 1 laminates, the damage is enveloped by a circle and so the selected points are fitted to that shape. The back side of the damage for this type is best approximated by a square, and so points fitted accordingly. However, for type 2 laminates, the damage on both the front and back of the impacted specimens is approximated by an enveloping circle. Dimensional data for damage is then extracted from the fitted circle/square and are provided in Table 2.

Table 2: Summary data from the impact force-time curves, damage sizes and spread angle

Parameter	Impact energy (Joules)	Units	Number of specimens	Type 1***	Type 2****
Average peak impact force	5	kN	3	1.93 ± 0.04	2.48 ± 0.02
Diameter of damage on top surface		mm		4.47 ± 0.21**	8.63 ± 1.69
Size of damage on bottom surface*		mm		10.97 ± 0.67	7.8 ± 1.93
Damage spread angle (α)		Deg		61.16	N/A
Average peak impact force	7.5	kN	3	2.02 ± 0.06	2.96 ± 0.02
Diameter of damage on top surface		mm		8.93 ± 0.15	9.23 ± 0.35
Size of damage on bottom surface*		mm		13.77 ± 1.36	9.03 ± 0.55
Damage spread angle (α)		Deg		53.44	N/A
Average peak impact force	10	kN	3	1.95 ± 0.06	3.27 ± 0.08
Diameter of damage on top surface		mm		12.13 ± 0.46	10.8 ± 1.15
Size of damage on bottom surface*		mm		18.5 ± 0.44	14.13 ± 1.71
Damage spread angle (α)		Deg		60.62	N/A

* is side of enveloping square for type 1 and diameter of enveloping circle for type 2

** The number after ± represents standard deviation

*** Theoretical stiffness values $E_{xx} = 48.46$ (GPa), $D_{11} = D_{22} = 20.72$ (kN.mm)

**** Theoretical stiffness values $E_{xx} = 40.50$ (GPa), $D_{11} = D_{22} = 33.45$ (kN.mm)

3.5 Mechanical shear test fixture

The impacted specimens were placed in a picture frame test fixture (see Figure 3). The specimens were held in place by clamping, 10 mm from all edges via four rails. The rails were bolted through to provide the gripping action on the specimen edges. A torque value of 40 kN.mm was used to tighten the rails. This setting provided a gauge dimension of 180 mm × 180 mm. The four corners of the fixture were pinned, allowing the pairs of rails to rotate relative to each other. During the test, the panel was subjected to shear by applying a pulling force to the diagonally opposed corners of the picture frame fixture. In this study, the pulling force was applied using a tensile INSTRON machine with load capacity of 100 kN at a speed of 2 mm/min.

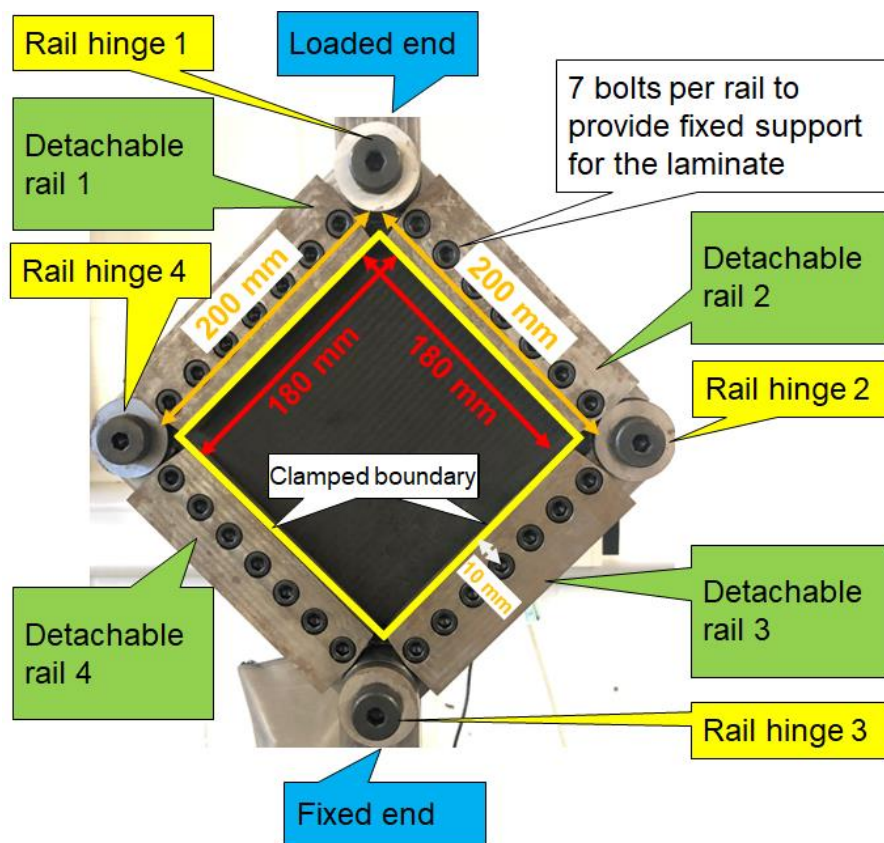


Figure 3: In-plane shear test set-up

4 Results and discussions

4.1 Drop weight impact analysis and damage size

The impact force-time (F-T) history curves for both type 1 and type 2 laminates are shown in Figure 4. The F-T curves for the type 1 laminates is characterised by six points *A*, *B*, *C*, *D*, *E* and *F*, compared to five points for the type 2. Furthermore, both laminate types demonstrated a double peak response, i.e. points *B* and *D*.

From point *A* to *B*, or otherwise known in the literature as the elastic region [29], the impact force increased approximately linearly with some oscillations that were more occurrent in type 1 than 2. These oscillations are attributed to matrix cracks that do not require significant energy or cause a noticeable drop in stiffness. The impact forces peaked at point *B* for both laminate types. The impact force at this point is known as a characteristic impact force, where the stiffness changes due to the Hertzian failure [30]. The value of peak forces were approximately 28%, 46% and 68% higher for type 2 than type 1, for energy levels 5 *J*, 7.5 *J* and 10 *J*, respectively. This is due to the higher bending stiffness (+61%) of the type 2 compared to type 1 laminates (see footnote of Table 2). It is also noted that, for each laminate type, the impact force increased with increasing impact energy as reported in [31]. However, the contact time did not alter significantly as the impact energy increased. This is contrary to the reports made by Aktas et al. [32], and can be explained by the higher impact energy levels in that study (40 *J*-50 *J*). It is further observed that, for both laminate types, the time at the peak contact force decreased with increasing impact energy confirming the findings of [32].

After point *B*, for both laminate types, discontinuities in the F-T signals were followed by oscillations and a sudden reduction (point *C*) in the force. This indicates the onset of delaminations, and noticeable change in stiffness. In other words, the

characteristic force at point *B* is regarded as a key indicator of a laminates ability to resist the initiation of delamination. It is noteworthy that the formation of damage such as delamination brought about the rapid decrease of the laminate's bending stiffness. This led to unloading of the specimen hence load reduction after the peak force point. Interestingly, a second peak point *D* was seen once the laminates started absorbing further impact force resulting from the impactors remaining potential energy. However, unlike type 2, the value of the second peak for type 1 was similar to that of the first peak. This could be indicative of the fact that whilst in-plane propagation of delamination was taking place, unlike type 2, thinner type 1 laminates were using more of their membrane stiffness to resist the out-of-plane impact forces. This is because membrane stiffness is not severely affected in the absence of fibre fracture.

From point *D* to *F* the potential energy of the impactor was transferred to the laminates. For type 1, the existence of point *E* indicates the perforation of the laminate.

As tabulated in Table 2, for both type 1 and type 2 laminates, the size of the damage on the front specimen face (impacted face) increased with increasing impact energy. For instance, the damage size of impact energy 10 *J* was 171% and 25% larger than 5 *J*, for type 1 and 2, respectively. However, the type 1 and 2 laminates demonstrated different behaviours in containing the damage through the thickness. In type 1, the size of the damage increased from the top surface to the bottom surface. On the other hand, for type 2, the GFRP ply on the impacted face endured larger damage compared to the type 1. Unlike type 1, the size of the damage on the back side of the type 2 laminates was smaller than the damage on the impacted face. This suggests that the GFRP plies on the top side of the laminates absorbed the impact energy and contained the damage.

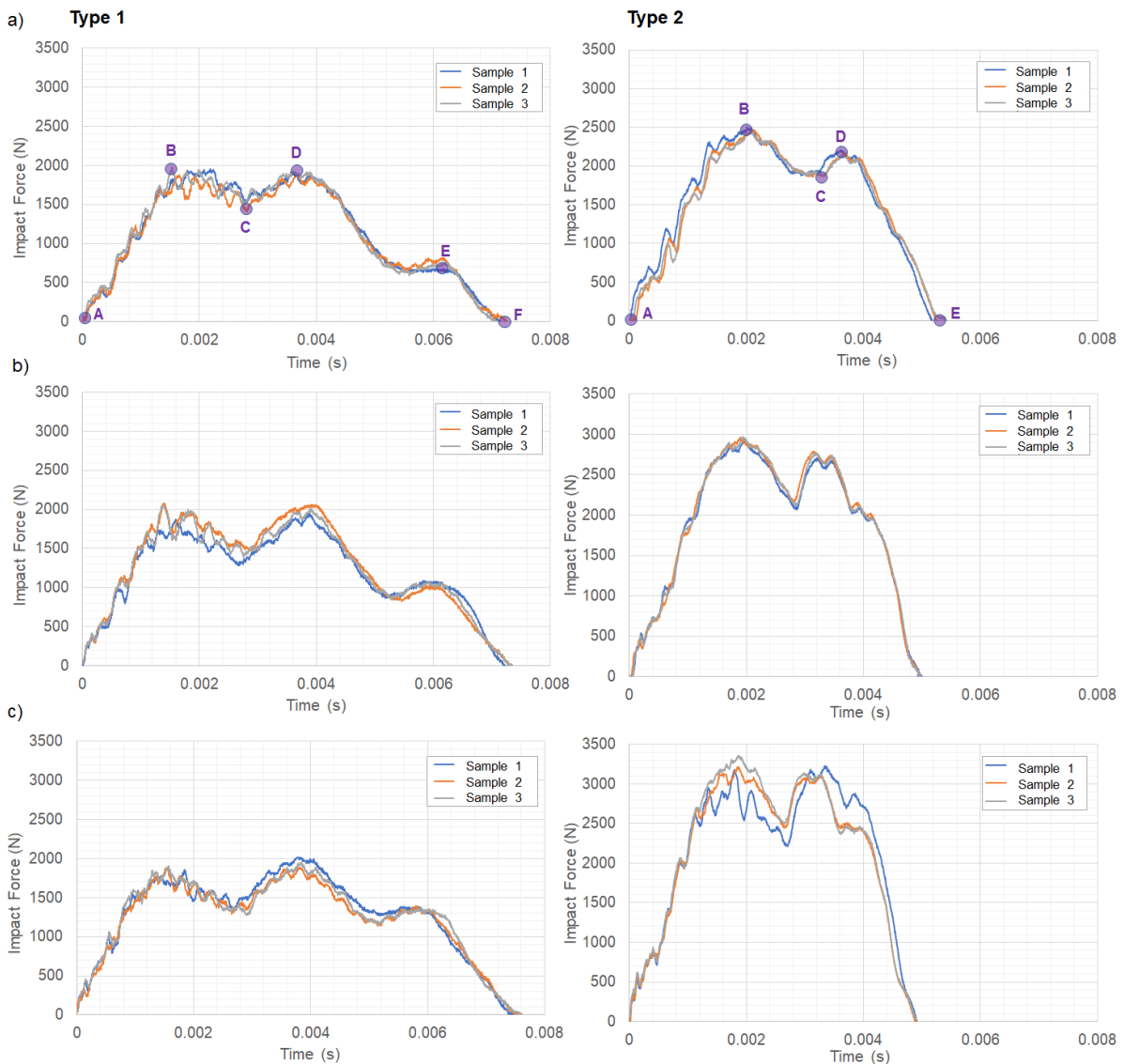


Figure 4: Impact load curves under energy levels a) 5 J, b) 7.5 J and c) 10 J for type 1 (left) and type 2 (right) laminates

The energy-time responses for both laminate types are shown in Figure 5 with characteristic information depicted on Figure 5a and summarised in Table 2. It is evident from the graphs that for each laminate type, the absorbed energy increased with increasing impact energy. A comparison of energy absorption between type 1 and 2 suggests that type 2 laminates absorbed $\approx 32\%$ and $\approx 8\%$ more energy for impact

levels 5 J and 7.5 J, respectively. However, for the highest impact energy, i.e. 10 J, the type 1 laminate absorbed $\approx 5\%$ more energy and less elastic energy than the type 2 laminate, see Figure 4c. This behaviour is a result of the significant fibre breakage and greater contact time of the impactor with the type 1 laminates (seen for all energy levels). These findings confirm those of [33].

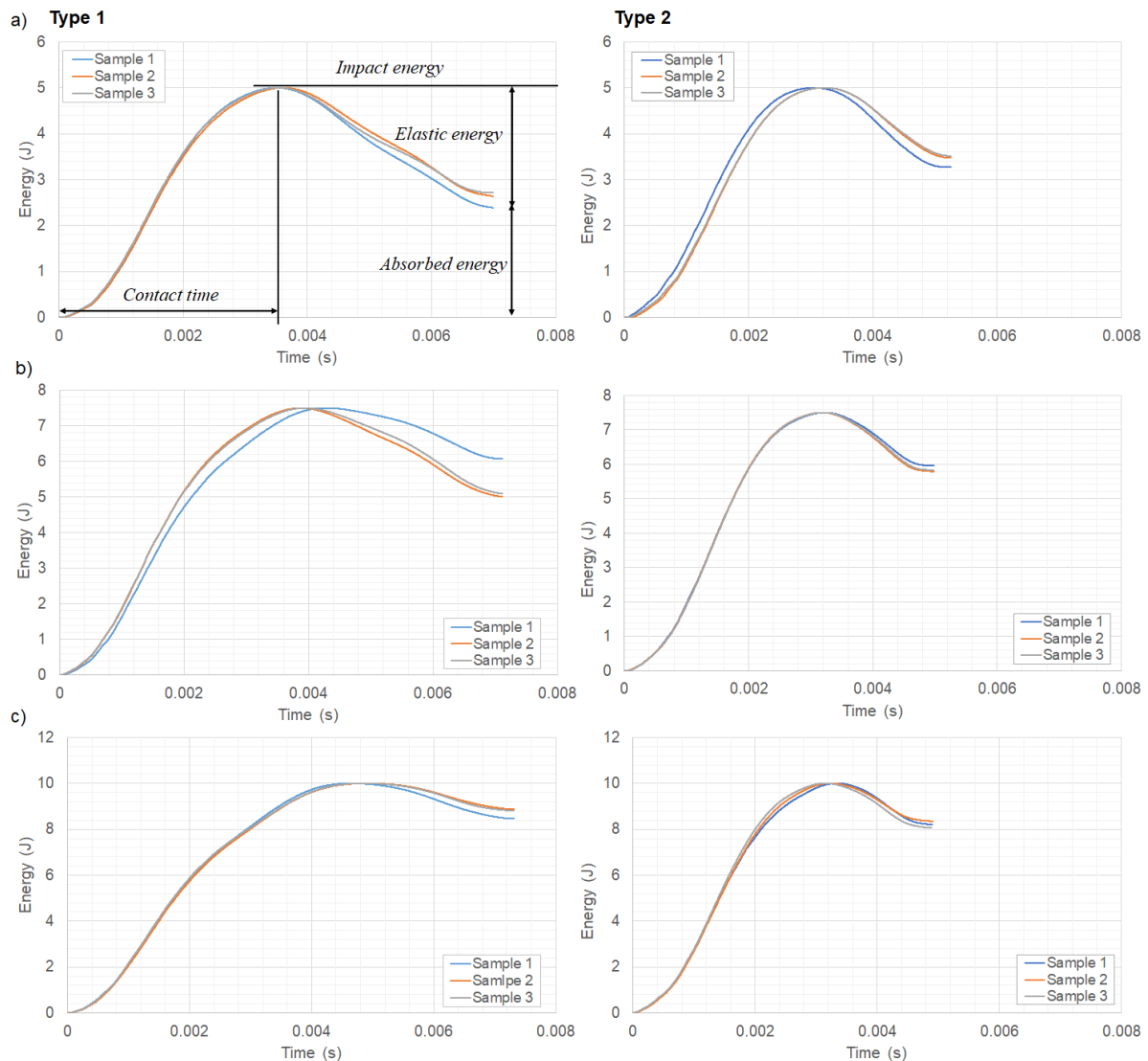


Figure 5: Energy versus time response for impact energies of a) 5 J, b) 7.5 J and c) 10 J for type 1 (left) and type 2 (right) laminates

A single specimen for each impact energy was sectioned at the centre of the impact. The samples were viewed under a microscope at a magnification factor of $\times 33$, as shown in Figure 6. For the type 1 laminates, the damage type comprised of

matrix cracks, delamination and, more importantly, considerable fibre fracture particularly at the bottom surface of the laminates. As impact energy level increased, the indentation depth increased. The type 2 laminates demonstrated superior performance for all energy levels in terms of damage. At lower energy levels of 5 J and 7.5 J, there was no through thickness damage. Therefore, it can be concluded that a hybrid of GFRP plies with X-shaped CFRP plies provided both adequate protection and stiffness levels to contain the damage to the surface, with negligible indentation depth. For the highest energy level of 10 J, matrix cracks and delaminations were visible but no fibre breakage took place. In other words, unlike type 1, type 2 laminates did not experience any spread of damage through the thickness. Figure 7 shows a schematic of typical damage mode in composite laminates resulting from low velocity impact. Generally, the delaminations may be assumed to be circular in shape and their size may be approximated to increase linearly from the top (impacted surface) to the bottom surface with a spread angle of α . Based on Table 2 and Figure 6, the spread angle did not apply to type 2 laminates as the through thickness damage was absent in the presence of protective GFRP plies. However, in type 1, the average spread angle across all impact energy levels were 58.40° showing various damage modes (as discussed above) through the thickness.

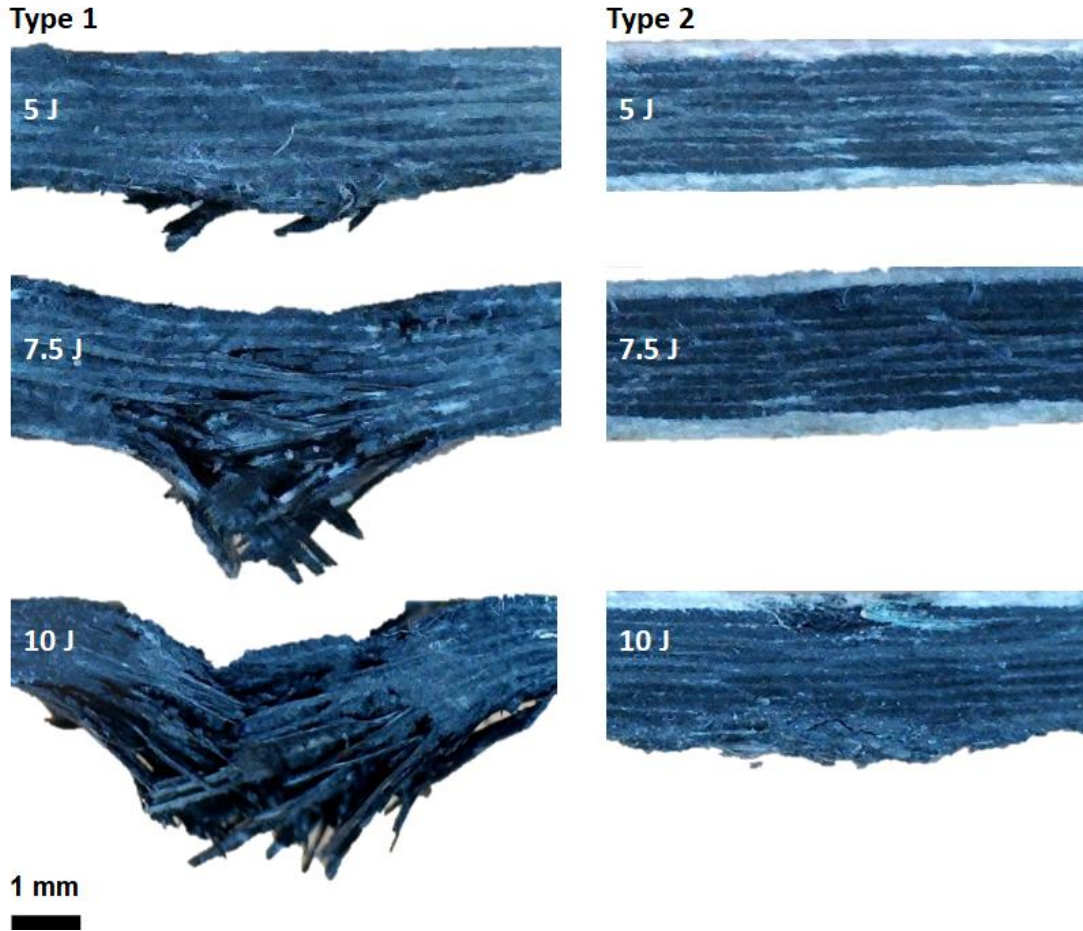


Figure 6: Cross sectional view of damage in type 1 (left) and type 2 (right) laminates after impact (scaled $\times 33$)

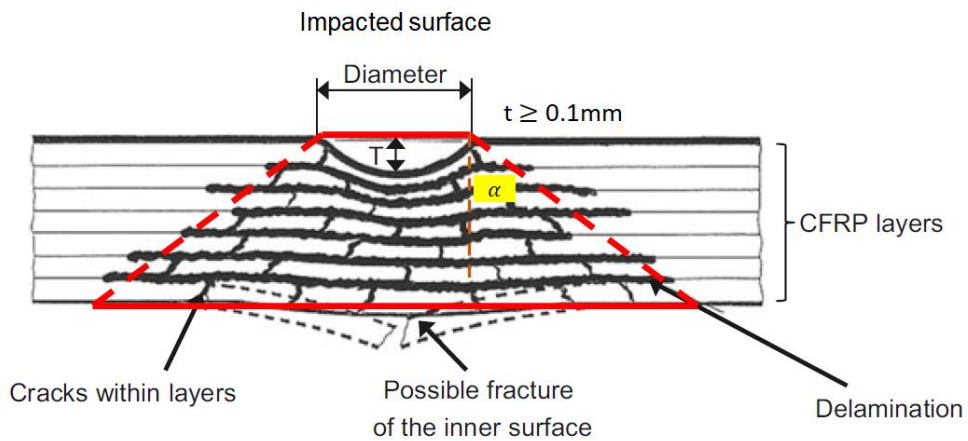


Figure 7: Schematic representation shows a typical impact damage mode for composite laminates with damage spread angle α

Figure 8 and Figure 9 show polarised and greyscale images of the impacted side of laminate types 1 and 2, respectively. The significance of such imaging techniques is that, if mounted on a drone or robot, an insight on the location of the damage on a large surface area such as an aircraft fuselage, wing or wind turbine blade can be acquired. This could be either via a human-assisted process, where fibre orientations are highlighted in images to aid manual defect detection, or via a form of machine learning method to automatically localise the defects. The authors developed and used a related technique in a previous work, which was aimed at non-contact repair quality assessment for highly loaded composite structures [28]. It is evident that as the impact energy increased, the damage detection rate improved as more disturbance in the polarised images took place. However, for physically smaller damage, the greyscale data still allowed the damaged region to be identified using a more subjective estimate of the points on the boundary of the damage. The results of damage size measurements are given in Table 2. As shown in Figure 9, the success of the technique is limited to CFRP since glass fibres did not polarise the light (disturbance in polarised images were not as pronounced as those for type 1) that requires further research. Again, however, measurements are still possible using a subjective analysis of the greyscale images. It is worth noting that health monitoring of GFRP material using optical techniques has been the focus of research in recent years. The reader is referred to [34] for further information.

Type 1

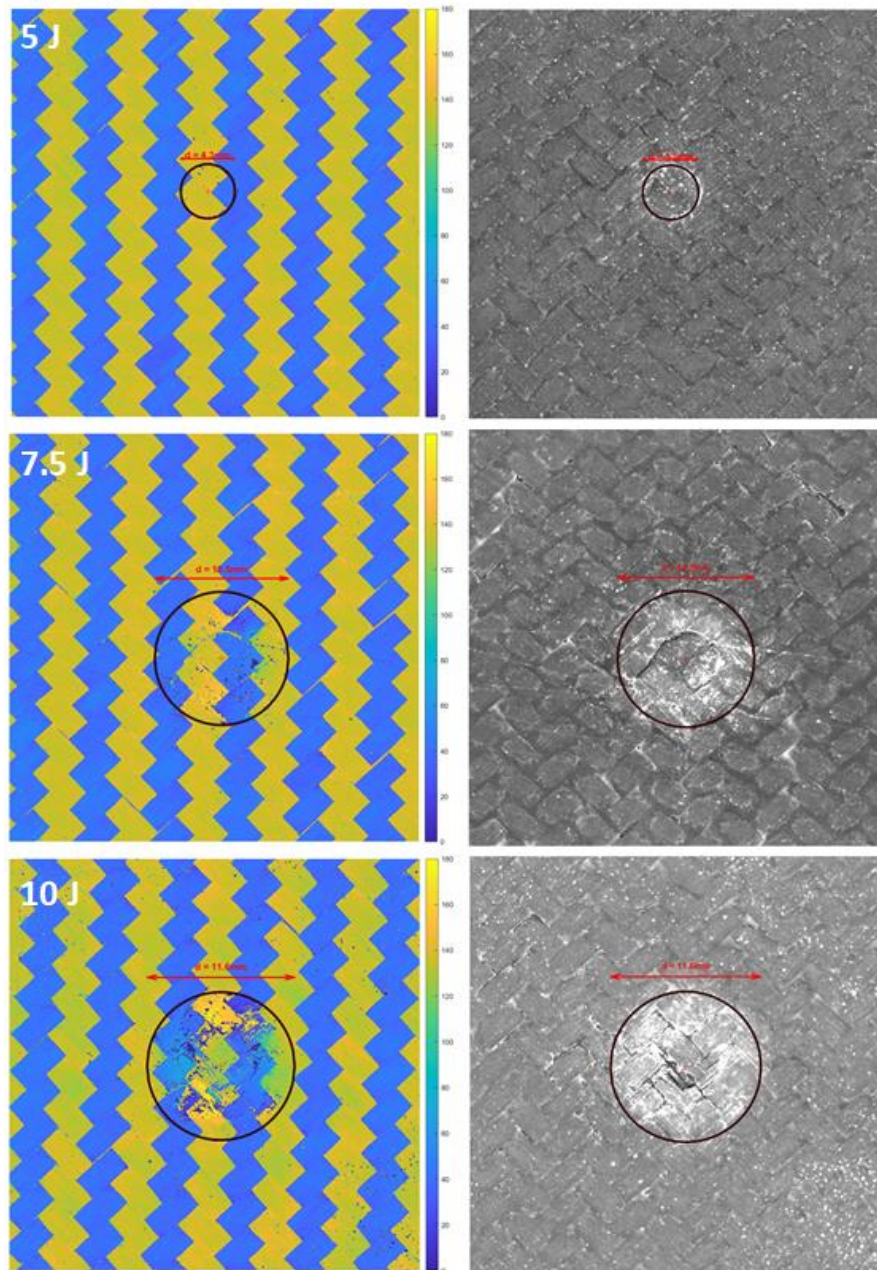


Figure 8: Polarised images (left) of type 1 impacted specimens and grey scale images (right) of damage for all impact energies. The diameter of damage is 4.3 mm, 10.5 mm and 11.6 mm for impact energies 5 J, 7.5 J and 10 J, respectively.

Type 2

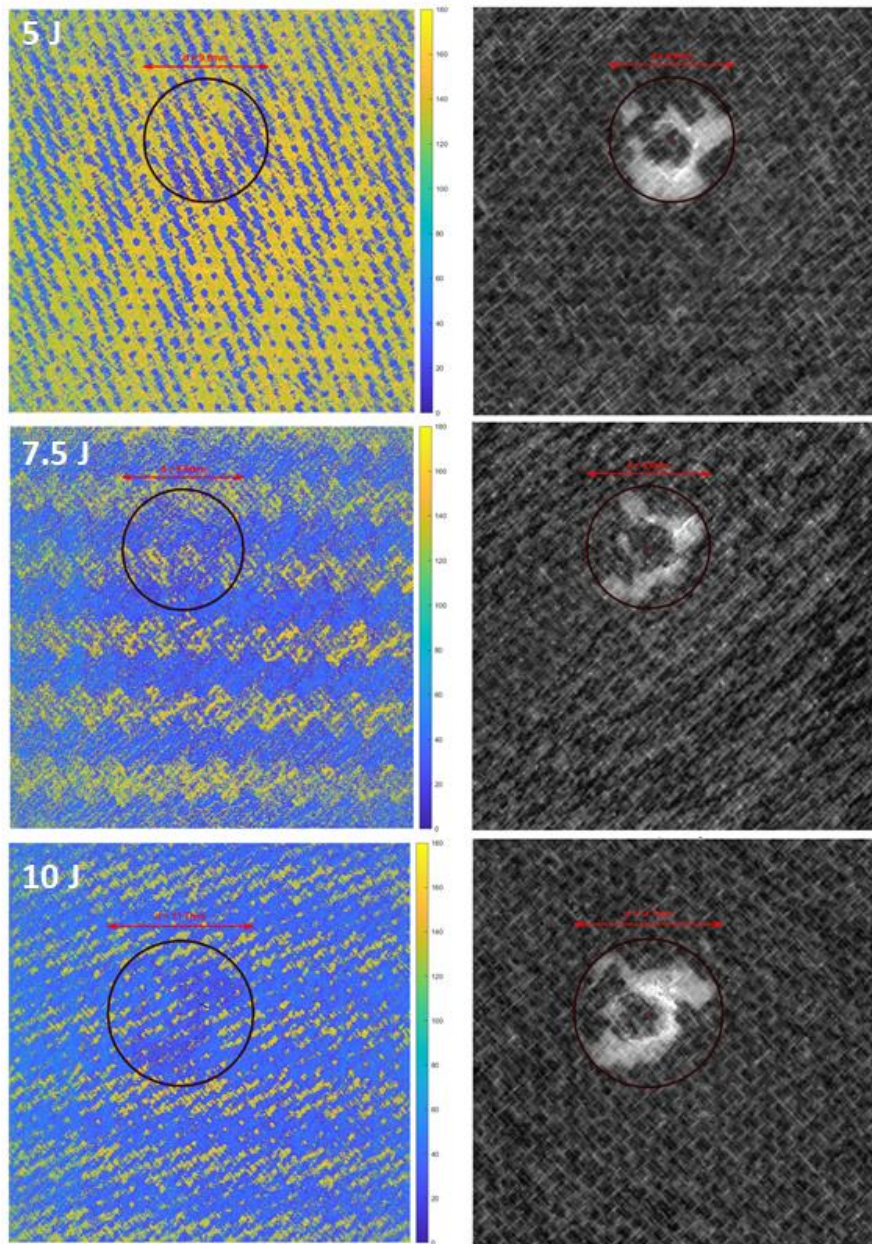


Figure 9: Polarised images (left) of type 2 impacted specimens and grey scale images (right) of damage for all impact energies. The diameter of damage is 9.8 mm, 9.6 mm and 11.7 mm for impact energies 5 J, 7.5 J and 10 J, respectively.

4.2 Load-displacement curves under quasi-static in-plane shear loading

(SAI tests)

Load-displacement graphs of the in-plane shear test after all impact energy levels for both laminate types are shown in Figure 10. Characteristic information of

these graphs such as buckling load, failure load and the slope of the linear portion of the graph are extracted and tabulated in Table 3. It is evident from the graphs that, as the impact energy level increases, the buckling load (purple point A of Figure 10), the failure load and the stiffness (slope of the linear portion of force-displacement graphs of Figure 10) for the two laminate types decreased marginally and commensurately.

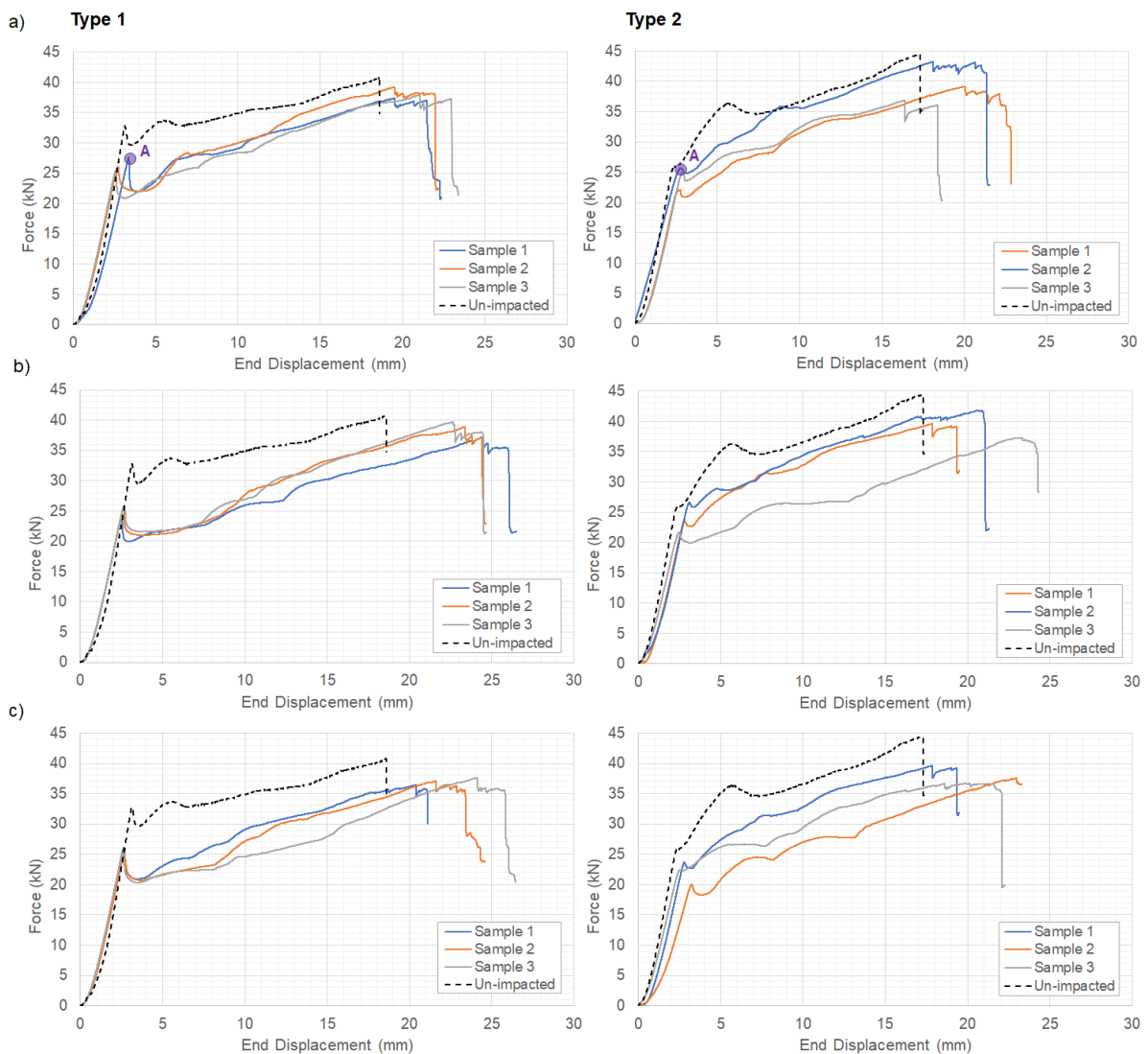


Figure 10: Force-displacement graphs after impact energies a) 5 J, b) 7.5 J and c) 10 J for type 1 (left) and type 2 (right) laminates. The black dashed line in all graphs is for pristine unimpacted specimens from study [11]

For the lower impact energies of 5 J and 7.5 J, the type 2 laminates showed \approx 12% and \approx 14% respective reduction in buckling load which is less than the \approx 19% and \approx 23% respective reduction for the type 1 laminates. However, the failure load in type 1 reduced by \approx 6%, \approx 5% and \approx 8% for impact energies of 5 J, 7.5 J and 10 J, respectively, whereas the reductions for type 2 were \approx 7%, \approx 10% and \approx 15%. The figures suggest that the GFRP plies were successful in reducing the impact damage of the type 2 laminate, leading to less reduction in the buckling load, but with less success in protecting the laminates post-buckling reserve. This is because the type 2 laminates had less membrane stiffness compared to type 1 (see Table 3) owing to the use of less stiff GFRP plies. It could be concluded that the buckling load is determined by the bending stiffness of the laminate whereas the failure load, in this study, is mostly affected by the membrane stiffness.

Table 3: Experimental buckling load, failure load and stiffness for all impact energies and laminate types

Laminate type	Impact Energy (J)	Number of specimens	Average buckling load (kN)	Average failure load (kN)	Stiffness (kN.mm)
Type 1	0*	1	32.00	40.63	15.80
	5	3	25.82 \pm 1.30**	38.20 \pm 0.93	11.91 \pm 0.73
	7.5	3	24.80 \pm 1.50	38.58 \pm 1.28	12.04 \pm 0.00
	10	3	25.36 \pm 0.60	37.05 \pm 0.61	11.99 \pm 0.26
Type 2	0*	2	27.90	43.94	14.23
	5	3	24.31 \pm 1.95	39.72 \pm 3.26	11.13 \pm 0.64
	7.5	3	23.98 \pm 2.61	39.59 \pm 2.28	11.77 \pm 0.26
	10	3	21.97 \pm 1.74	37.09 \pm 2.35	10.90 \pm 1.25

* refer to study [11]

** \pm represents the standard deviation

Figure 11 plots the ratio of failure to buckling load of the present study along with ratios of stiffness of impacted specimens versus un-impacted pristine specimens [11]. Based on the figure, for type 2 laminates, the failure to buckling load ratio increased consistently as the impact energy levels increased, but the ratio showed less sensitivity when compared to type 1 laminates. Furthermore, in type 2 laminates, stiffness reduction after impact was less compared to type 1.

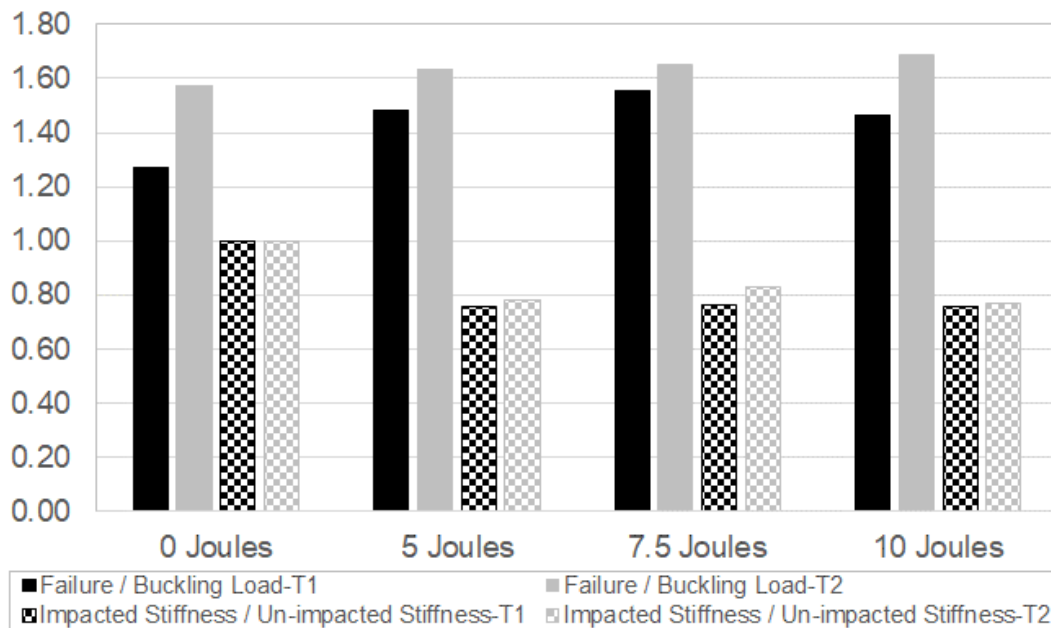


Figure 11: Comparison of failure to buckling load and stiffness ratio of impacted specimen for each laminate type with those of un-impacted pristine laminates of [11]. The values are normalised to those of un-impacted specimens.

Figure 12 shows both the deformed shape and the fracture path of type 1 laminates under shear loading after various graduated impact energies. It is evident that, for low energy levels of 5 J and 7.5 J, the laminates after impact deformed in a mode 1 shape (yellow dashed lines) and continued to fail with fracture along the main diagonal direction (red lines), i.e. in the direction of tensile loading. This is similar to the fracture path seen for pristine laminate [11]. However, for the higher impact energy (10 J) the laminates started deforming in a mode 1 shape (yellow dashed line of Figure

12c), but this was followed with a local buckling shape (orange dashed line of Figure 12c) as a result of delamination in the impacted zone. Furthermore, the fracture path extended from the main diagonal to the diagonal direction perpendicular to the loading direction [25].

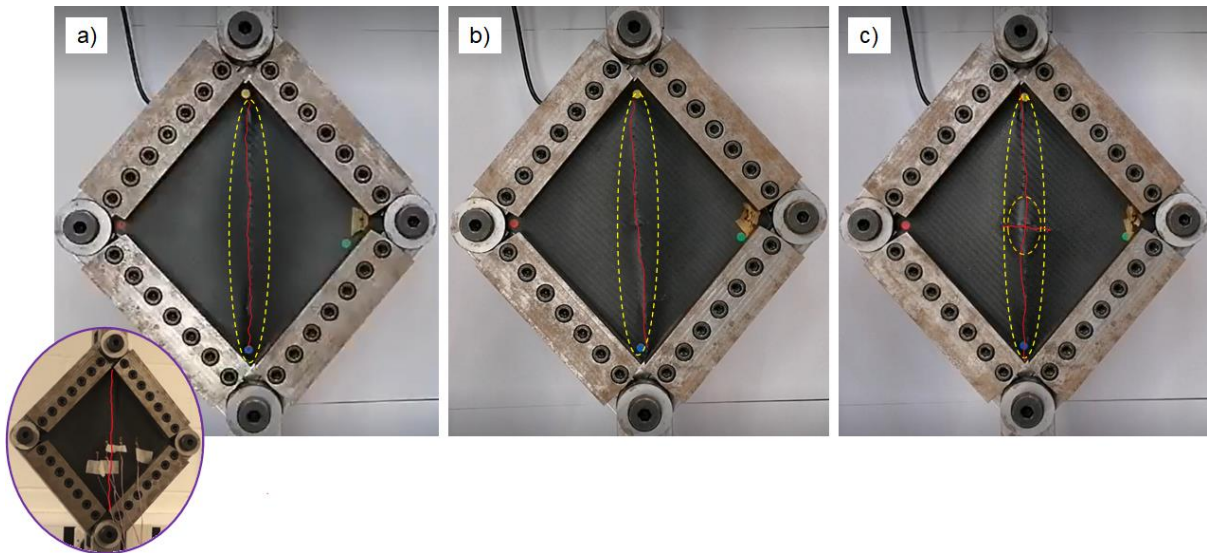


Figure 12: Deformed shape and fracture path of type 1 laminates under shear load after impact energy levels; a) 5 J, b) 7.5 J and c) 10 J (small picture on the left bottom is for pristine laminates of study [11])

Figure 13 shows both the deformed shape and the fracture path of the type 2 laminates under in-plane shear loading. For the low energy levels of 5 J and 7.5 J, the laminates after impact deformed in a mode 2 shape (yellow dashed lines) of the pristine laminates and continued to fail with two sequential fracture paths. The first fracture path was similar to the pristine laminates [11], in which failure occurred at an offset from the main diagonal at the location of GFRP ply drop offs. This was then followed immediately by the second fracture path along the main diagonal direction. Based on the previous study, the second fracture path was not present in the pristine laminates. This observation suggests that the impact phenomenon altered the initial imperfection as a pre-cursor for buckling and mode shape deformation in the post-

buckling regime. This is in agreement with the findings of Ghelli et al. [35]. It should be noted that due to the protective action of the GFRP plies, unlike type 1, no delamination and hence no sublaminates buckling was present during the experiment.

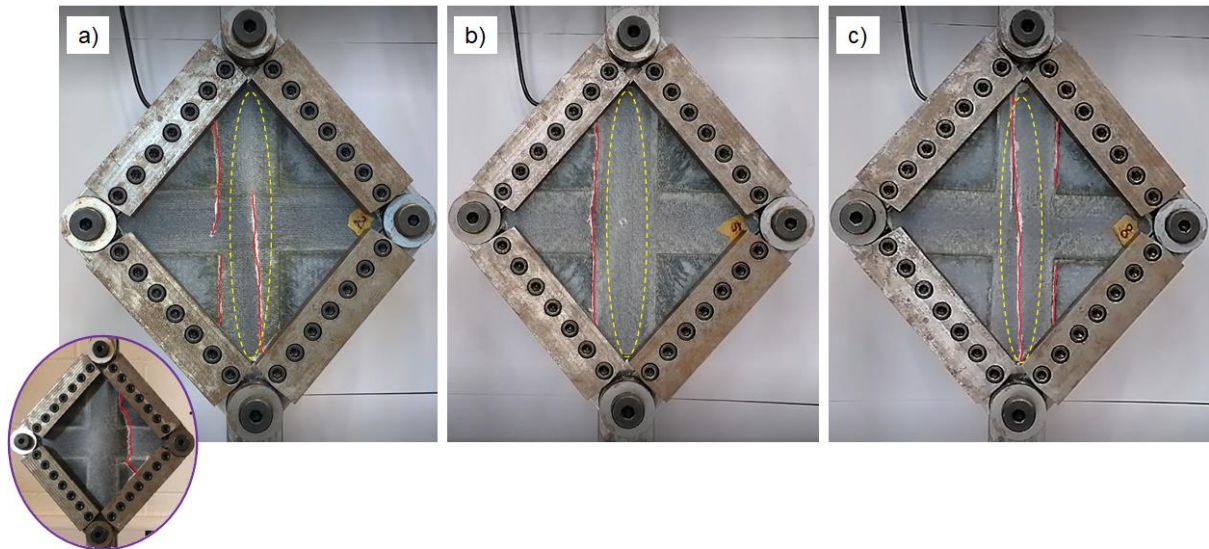


Figure 13: Deformed shape and fracture path of type 2 laminates under shear load after impact energy levels; a) 5 J, b) 7.5 J and c) 10 J (small picture on the left bottom is for pristine laminates of study [11])

5 Conclusions

Buckling and post-buckling performance of pure twill woven CFRP (type 1) and a novel X-braced hybrid laminate design (type 2) after graduated impact energies were investigated experimentally, considering pure in-plane shear loading. It was shown that type 1 laminates went through significant damage after impact (VID) including matrix crack, delamination and fibre breakage. On the other hand, the type 2 laminates experienced BVID with no through thickness damage thanks to protective GFRP plies. Also, the type 2 laminates had higher peak impact forces than those seen by the type 1 design. Type 2 laminates experienced higher peak impact forces of 28%, 46% and 68% for energy levels 5 J, 7.5 J and 10 J, respectively, compared to type 1. Additionally, the type 2 laminates absorbed more energy than the type 1 laminates for low energy

impacts (5 J, 7.5 J). However, as the impact energy increased to 10 J, the type 1 laminates absorbed $\approx 5\%$ more energy than the type 2 laminates. This behaviour is a direct result of a greater volume of fibre damage when the type 2 laminates are subjected to the higher impact energy. Novel machine vision techniques successfully identified damage location and measured damage size for type 1 laminates, however the technique was not as successful for type 2 laminates. This was due to GFRP plies' inability to significantly polarise the emitted light. The buckling and post-buckling performance study showed that buckling load, failure load and laminate stiffness reduced because of graduated impacts. The buckling load of type 2 reduced less than type 1 but the reduction of failure load was more than that of type 1. However, the stiffness reduction was insensitive to the impact energy level. It was shown that after the graduated impacts, both laminate types followed a stable load-displacement graph under in-plane shear loading. It is worth noting that the studied laminate designs showed an average of 1.5 and 1.66 failure to buckling shear load ratio after the impact phenomenon compared to pristine values of 1.27 and 1.57, for type 1 and 2 respectively. This demonstrates a superior resilience of the type 2 laminates. Additionally, the impact phenomenon had an influence on the initial imperfection of the type 2 laminates. This led to a second fracture path along the main diagonal direction which did not exist in the pristine laminates. However, the fracture path of both impacted and pristine type 1 laminates were similar.

6 CRediT authorship contribution statement

Mahdi Damghani: Conceptualisation, Methodology, Validation, Formal analysis, Resources, Writing - original draft, Writing- review & editing, Visualisation, Supervision, Project administration. **John Sadler:** Investigation, Data curation. **Ethan Sammon:** Investigation, Data curation. **Gary Atkinson:** Formal analysis, Resources,

Writing- review & editing, Visualisation. **Jason Matthews:** Resources. **Adrian Murphy:** Writing -original draft, Writing - review & editing.

7 Declaration of conflicting interests

The authors declared no potential conflicts of interest with respect to the research, authorship, and/or publication of this article.

8 Acknowledgment

The authors express their gratitude to Douglas Nash and Daniel Cole (technicians at UWE) for their assistance and facilitating the research.

9 References

- [1] N. R. Kolanu, G. Raju, and R. M., "Post-buckling failure studies on quasi-isotropic CFRP panels under positive and negative in-plane shear loading," *Composite Structures*, vol. 246, p. 112379, 2020, doi: <https://doi.org/10.1016/j.compstruct.2020.112379>.
- [2] S. Fotouhi, S. Khayatzadeh, W. Pui Xia, M. Damghani, M. Bodaghi, and M. Fotouhi, "Detection of Barely Visible Impact Damage in Polymeric Laminated Composites Using a Biomimetic Tactile Whisker," *Polymers (Basel)*, vol. 20, no. 13, p. 3587, 2021, doi: <https://doi.org/10.3390/polym13203587>.
- [3] J. M. Koo, J. H. Choi, and C. S. Seok, "Prediction of post-impact residual strength and fatigue characteristics after impact of CFRP composite structures," *Composites Part B: Engineering*, 2014, doi: [10.1016/j.compositesb.2014.01.024](https://doi.org/10.1016/j.compositesb.2014.01.024).

- [4] W. J. Cantwell and J. Morton, "Geometrical effects in the low velocity impact response of CFRP," *Composite Structures*, vol. 12, pp. 39–59, 1989, doi: 10.1016/0263-8223(89)90043-3.
- [5] M. Fotouhi, M. Damghani, M. C. Leong, S. Fotouhi, M. Jalalvand, and M. R. Wisnom, "A comparative study on glass and carbon fibre reinforced laminated composites in scaled quasi-static indentation tests," *Composite Structures*, vol. 245, p. 112327, 2020, doi: 10.1016/j.compstruct.2020.112327.
- [6] I. Kondakov, A. Chernov, N. Guseva, and M. Levchenkov, "Protective elements for lattice composite fuselage structures against low-velocity impacts," *Aerospace Systems*, vol. 5, no. 1, pp. 1–9, 2022, doi: 10.1007/s42401-022-00130-4.
- [7] F. Romano, F. di Caprio, and U. Mercurio, "Compression after Impact Analysis of Composite Panels and Equivalent Hole Method," *Procedia Engineering*, vol. 167, pp. 182–189, Jan. 2016, doi: 10.1016/J.PROENG.2016.11.686.
- [8] P. Rozylo, H. Debski, and T. Kubiak, "A model of low-velocity impact damage of composite plates subjected to Compression-After-Impact (CAI) testing," *Composite Structures*, vol. 181, pp. 158–170, 2017, doi: <https://doi.org/10.1016/j.compstruct.2017.08.097>.
- [9] M. Damghani, N. Ersoy, M. Piorkowski, and A. Murphy, "Experimental evaluation of residual tensile strength of hybrid composite aerospace materials after low velocity impact," *Composites Part B: Engineering*, vol. 179, p. 107537, Dec. 2019, Accessed: Nov. 06, 2019. [Online]. Available: <https://www.sciencedirect.com/science/article/abs/pii/S1359836819337631>

- [10] W. Li and H. Nie, "Predicting post-impact compression strength of composite structures using the inverse method," *Composite Structures*, vol. 245, p. 112348, 2020, doi: <https://doi.org/10.1016/j.compstruct.2020.112348>.
- [11] M. Damghani, C. Wallis, J. Bakunowicz, and A. Murphy, "Using laminate hybridisation (CFRP-GFRP) and shaped CFRP plies to increase plate post-buckling strain to failure under shear loading," *Thin-Walled Structures*, vol. 162, p. 107543, 2021, doi: <https://doi.org/10.1016/j.tws.2021.107543>.
- [12] F. Chen, W. Yao, and W. Jiang, "Experimental and simulation investigation on BVID and CAI behaviors of CFRP laminates manufactured by RTM technology," *Engineering Computations*, vol. 38, no. 5, pp. 2252–2273, Jan. 2021, doi: [10.1108/EC-01-2020-0008](https://doi.org/10.1108/EC-01-2020-0008).
- [13] B. Ostré, C. Bouvet, C. Minot, and J. Aboissièrè, "Experimental analysis of CFRP laminates subjected to compression after edge impact," *Composite Structures*, vol. 152, pp. 767–778, Sep. 2016, doi: [10.1016/J.COMPSTRUCT.2016.05.068](https://doi.org/10.1016/J.COMPSTRUCT.2016.05.068).
- [14] J. Zou *et al.*, "Damage and failure analysis of composite stiffened panels under low-velocity impact and compression after impact," *Composite Structures*, vol. 262, p. 113333, Apr. 2021, doi: [10.1016/J.COMPSTRUCT.2020.113333](https://doi.org/10.1016/J.COMPSTRUCT.2020.113333).
- [15] ASTM D7136, *Standard Test Method for Measuring the Damage Resistance of a Fiber-Reinforced Polymer Matrix Composite to a Drop-Weight Impact Event*. West Conshohocken, Pennsylvania: ASTM International, 2015.
- [16] X. C. Sun and S. R. Hallett, "Failure mechanisms and damage evolution of laminated composites under compression after impact (CAI): Experimental and

- numerical study,” *Composites Part A: Applied Science and Manufacturing*, vol. 104, pp. 41–59, 2018, doi: <https://doi.org/10.1016/j.compositesa.2017.10.026>.
- [17] H. Tuo, Z. Lu, X. Ma, C. Zhang, and S. Chen, “An experimental and numerical investigation on low-velocity impact damage and compression-after-impact behavior of composite laminates,” *Composites Part B: Engineering*, vol. 167, pp. 329–341, Jun. 2019, doi: [10.1016/J.COMPOSITESB.2018.12.043](https://doi.org/10.1016/J.COMPOSITESB.2018.12.043).
- [18] A. Gliszczyński, R. Bogenfeld, R. Degenhardt, and T. Kubiak, “Corner impact and compression after impact (CAI) of thin-walled composite profile – An experimental study,” *Composite Structures*, vol. 248, p. 112502, Sep. 2020, doi: <https://doi.org/10.1016/j.compstruct.2020.112502>.
- [19] C. Zhang and K. T. Tan, “Low-velocity impact response and compression after impact behavior of tubular composite sandwich structures,” *Composites Part B: Engineering*, vol. 193, p. 108026, Jul. 2020, doi: [10.1016/J.COMPOSITESB.2020.108026](https://doi.org/10.1016/J.COMPOSITESB.2020.108026).
- [20] J. A. Wu, Z. Zhang, X. Dai, L. Duan, Y. Lin, and M. Sun, “Effect of stacking sequence on multi-point low-velocity impact and compression after impact damage mechanisms of UHMWPE composites,” *Polymer Composites*, vol. 42, no. 12, pp. 6500–6511, 2021, doi: <https://doi.org/10.1002/pc.26316>.
- [21] A. Malhotra and F. J. Guild, “Impact Damage to Composite Laminates: Effect of Impact Location,” *Applied Composite Materials*, vol. 21, no. 1, pp. 165–177, 2014, doi: [10.1007/s10443-013-9382-z](https://doi.org/10.1007/s10443-013-9382-z).
- [22] R. Bogenfeld, P. Schmiedel, N. Kuruvadi, T. Wille, and J. Kreikemeier, “An experimental study of the damage growth in composite laminates under

- tension–fatigue after impact,” *Composites Science and Technology*, vol. 191, p. 108082, May 2020, doi: 10.1016/J.COMPSCITECH.2020.108082.
- [23] Y. Feng, Y. He, X. Tan, T. An, and J. Zheng, “Experimental investigation on different positional impact damages and shear-after-impact (SAI) behaviors of stiffened composite panels,” *Composite Structures*, vol. 178, pp. 232–245, Oct. 2017, doi: 10.1016/J.COMPSTRUCT.2017.06.053.
- [24] Y. Feng, Y. He, X. Tan, T. An, and J. Zheng, “Investigation on impact damage evolution under fatigue load and shear-after-impact-fatigue (SAIF) behaviors of stiffened composite panels,” *International Journal of Fatigue*, vol. 100, pp. 308–321, Jul. 2017, doi: 10.1016/J.IJFATIGUE.2017.03.046.
- [25] O. E. Oluwabusi and E. A. Toubia, “Effect of central circular cut-out and low velocity impact damage on shear buckling and post-buckling of composite laminated plates,” *Composite Structures*, vol. 245, p. 112304, Aug. 2020, doi: 10.1016/J.COMPSTRUCT.2020.112304.
- [26] M. Damghani, R. A. Pir, A. Murphy, and M. Fotouhi, “Experimental and numerical study of hybrid (CFRP-GFRP) composite laminates containing circular cut-outs under shear loading,” *Thin-Walled Structures*, vol. 179, p. 109752, 2022, doi: <https://doi.org/10.1016/j.tws.2022.109752>.
- [27] G. A. Atkinson, S. O. Nash, and L. N. Smith, “Precision fibre angle inspection for carbon fibre composite structures using polarisation vision,” *Electronics (Basel)*, vol. 22, no. 10, p. 2765, 2021, doi: 10.3390/electronics10222765.
- [28] M. Damghani *et al.*, “Design, novel quality check and experimental test of an original variable length stepped scarf repair scheme,” *Composites Part B:*

- Engineering*, vol. 230, p. 109542, Feb. 2022, doi: 10.1016/J.COMPOSITESB.2021.109542.
- [29] J. Zhou, B. Liao, Y. Shi, Y. Zuo, H. Tuo, and L. Jia, "Low-velocity impact behavior and residual tensile strength of CFRP laminates," *Composites Part B: Engineering*, vol. 161, pp. 300–313, 2019, doi: <https://doi.org/10.1016/j.compositesb.2018.10.090>.
- [30] E. Panettieri, D. Fanteria, M. Montemurro, and C. Froustey, "Low-velocity impact tests on carbon/epoxy composite laminates: A benchmark study," *Composites Part B: Engineering*, vol. 107, pp. 9–21, 2016, doi: <https://doi.org/10.1016/j.compositesb.2016.09.057>.
- [31] K. I. I. Ismail, M. T. H. T. H. Sultan, A. U. M. U. M. Shah, M. Jawaid, and S. N. A. N. A. Safri, "Low velocity impact and compression after impact properties of hybrid bio-composites modified with multi-walled carbon nanotubes," *Composites Part B: Engineering*, vol. 163, pp. 455–463, Apr. 2019, doi: <https://doi.org/10.1016/j.compositesb.2019.01.026>.
- [32] M. Aktas, R. Karakuzu, and B. M. Icten, "Impact Behavior of Glass/Epoxy Laminated Composite Plates at High Temperatures," *Journal of Composite Materials*, vol. 44, no. 19, pp. 2289–2299, May 2010, doi: 10.1177/0021998310369576.
- [33] S. Kannivel, H. Subramanian, V. Arumugam, and H. N. Dhakal, "Low-Velocity Impact Induced Damage Evaluation and Its Influence on the Residual Flexural Behavior of Glass/Epoxy Laminates Hybridized with Glass Fillers," *Journal of Composites Science*, vol. 4, no. 3. 2020. doi: 10.3390/jcs4030099.

- [34] G. Hegedűs, T. Sarkadi, and T. Czigány, "Analysis of the Light Transmission Ability of Reinforcing Glass Fibers Used in Polymer Composites," *Materials*, vol. 10, no. 6. 2017. doi: 10.3390/ma10060637.
- [35] D. Ghelli and G. Minak, "Low velocity impact and compression after impact tests on thin carbon/epoxy laminates," *Composites Part B: Engineering*, vol. 42, no. 7, pp. 2067–2079, 2011, doi: <https://doi.org/10.1016/j.compositesb.2011.04.017>.